MODELING OF THE 1939 ERZINCAN (Ms~7.8) EARTHQUAKE: OBSERVATIONS ON ANTICIPATED GROUND MOTIONS AND DAMAGE DISTRIBUTION

S. Karimzadeh[1] and A. Askan[2]

[1] *Post-doctoral Researcher, Civil Eng. Department, Middle East Technical University, Turkey*
[2] *Prof. Dr., Civil Eng. Department, Middle East Technical University, Turkey*
Email: shaghkn@gmail.com

ABSTRACT:

Located within a pull-apart basin at the conjunction of three active faults (North Anatolian, North East Anatolian and Ovacik Faults), Erzincan city center is one of the most hazardous regions in the world. Combination of the seismotectonic and geological settings of the region has resulted in series of significant seismic activities including the 27 December 1939 (Ms~7.8) and the 13 March 1992 (Mw=6.6) events. The former earthquake was in the pre-instrumental era in the region with no available local seismograms. However, despite the sparse local network, the 1992 earthquake has been studied extensively. The objective of this study is to model the 1939 Erzincan earthquake using the regional seismic and geological parameters available mostly from the previous studies on the 1992 event. Despite several uncertainties involved, such an effort to quantitatively simulate the 1939 earthquake is promising, given the historical reports of extensive damage and fatalities in the area. The results are expressed in terms of anticipated spatial distribution of selected ground motion parameters and felt-intensity maps in the region. These shaking maps are obtained using local correlations between intensity and peak ground motion values. Comparisons of simulated motions against empirical prediction equations and the existing damage observations indicates a reasonable modeling of the 1939 earthquake.

KEYWORDS: The 1939 Erzincan, Ground motion simulation, Felt intensity, Seismic damage

1. INTRODUCTION

Study of historical events without recorded ground motion data is challenging yet promising particularly if the earthquake is large and destructive. Ground motion simulations can be performed for such historical events to obtain the anticipated ground motions in the corresponding meizoseismal areas. Since a direct validation of the simulated data with the recorded data is not possible for historical earthquakes, indirect validations of the simulations can be performed in terms of comparisons with the shaking intensity distributions or empirical ground motion prediction equations.

In this study, an initial attempt is presented to simulate the 1939 Erzincan earthquake (Ms~7.8) which is among the most destructive events of the last century causing a surface rupture length of 360 km on five different segments on North Anatolian Fault Zone (NAFZ). The earthquake caused significant damage to about 120,000 buildings in the city and resulted in more than 30,000 fatalities (Barka 1996). In the aftermath of the event, the city was relocated towards North. The region has always been seismically active due to its tectonic nature: Historical records indicate approximately twenty large earthquakes close to Erzincan within the past 1000 years (Barka, 1993). In addition to the 1939 earthquake, Erzincan experienced another destructive event in 1992 (Mw=6.6) which caused major structural loss yielding a large number of fatalities. Even though the 1992 event is simulated in previous studies (Askan et al., 2013; 2015; 2017), a quantified ground motion model of the1939 earthquake is not available. In this paper, a preliminary simulation is performed using the path and site parameters verified with

the strong motion records of the 1992 event along with the anticipated source parameters of the 1939 event from observations and other studies (Barka, 1996; Stein et al., 1997; Askan et al. 2013; Gursoy et al., 2013). Simulated motions are initially compared with ground motion prediction equations. Then, the spatial distribution of the simulated peak ground motion parameters are converted into intensity values in order to compare with the observed intensity distribution of the 1939 event as presented in Altinok and Ersoy (2000).

2. STUDY REGION AND INFORMATION ON THE EVENT

The most destructive earthquakes in Turkey have occurred on the NAFZ which is one of the most active fault zones in the world. During the last century, several major events occurred along this fault zone starting with the 1939 Erzincan (Ms~7.8) event and moved westwards (e.g.: Ambraseys, 1970; Barka, 1992; Barka, 1996; Stein et al., 1997; Armijo et al., 2002). Most of the previous studies in Turkey have focused on the western parts of NAFZ due to the industrial facilities and dense population there. Yet, the Eastern sections of NAFZ including Erzincan, should also be studied in detail due to the intense regional seismic activity. Such efforts are particularly necessary not only to investigate the past earthquakes in the region but also for risk mitigation in potential large earthquakes.

This study focuses on the Erzincan city center and its surroundings within a selected mesh bounded by 39º-40ºN latitudes and 39º-40ºE longitudes. Erzincan is located on an alluvium pull-apart basin. The seismic activity arise from the complex tectonics regime: The left-lateral strike slip Ovacik Fault and the North East Anatolian Faults intersect the right-lateral North Anatolian Fault at the southern and northern edge of the Erzincan Basin, respectively (e.g.: Bernard et al., 1997; Avsar et al., 2013) as shown in Figure 1.

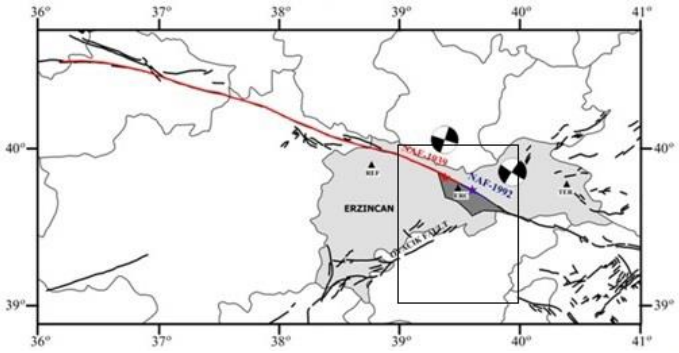

Figure 1. Seismotectonics in the Erzincan region with the fault systems and the epicenters of the 1939 and 1992 events. The light grey region is the Erzincan county and the dark grey area is the Erzincan basin where the historical and the current city center is located. The rectangle box shows the study area (Figure is adapted from Askan et. al. 2017).

3. SIMULATION OF THE 1939 ERZINCAN (Ms~7.8) EARTHQUAKE

With the advance of computers and mathematical models, simulation methods have been developed to obtain reliable synthetic ground motion records by modeling the earthquake source, path and site effects. As the two main approaches, deterministic and stochastic models are used frequently: Deterministic approach, which requires well defined source and velocity models, provides numerical solutions of the wave equation (e.g.: Frankel, 1993; Olsen et al., 1996). It is physical and accurate but practical only up to certain frequencies due to the minimum wavelength requirement. Stochastic approach models the ground motions as a combination of the far field S-wave spectrum and random phase angles (Boore, 1983; Beresnev and Atkinson, 1997). It models the higher frequencies effectively despite the lack of full wave propagation and complex source effects (e.g.: Castro et al., 2001; Motazedian and Moinfar, 2006; Askan et al, 2013; 2015; 2017; Karimzadeh et al, 2017a; 2017b). In this study, stochastic approach is preferred since there is neither a detailed source model nor any recorded seismograms of the 1939 Erzincan earthquake.

Stochastic finite-fault method used in this study models ground motions radiating from a rectangular finite-fault discretized into subfaults each of which is a stochastic point source with an ω^{-2} spectrum. The hypocenter is located on one of the subfaults and the rupture is assumed to start propagating radially from the hypocenter with a constant rupture velocity. Each subfault is triggered when the rupture reaches the center of that subfault. The contribution of all subfaults is summed with appropriate time delays in order to obtain the entire fault plane's contribution to the seismic field at any observation point. In the dynamic corner frequency concept, the total energy radiated from the fault is conserved regardless of the selected subfault size. In this study, we use the dynamic corner frequency approach as implemented in the computer program EXSIM (Motazedian and Atkinson, 2005).

In the dynamic corner frequency approach, the acceleration spectrum $A_{ij}(f)$ of the ij^{th} subfault is expressed in terms of source, path and site effects as follows:

$$A_{ij}(f) = CM_{0ij}H_{ij}\frac{(2\pi f)^2}{\left[1+\left(\frac{f}{f_{c_{ij}}}\right)^2\right]}e^{-\frac{\pi f R_{ij}}{Q(f)\beta}}G(R_{ij})A(f)e^{-\pi\kappa f} \quad (1)$$

where $C = \frac{\mathfrak{R}^{\theta\varphi}\cdot\sqrt{2}}{4\pi\rho\beta^3}$ is a scaling factor, $\mathfrak{R}^{\theta\varphi}$ is the radiation pattern, ρ is the density, β is the shear-wave velocity, $M_{0_{ij}} = \frac{M_0 S_{ij}}{\sum_{k=1}^{nl}\sum_{l=1}^{nw} S_{kl}}$ is the seismic moment, S_{ij} is the relative slip weight and $f_{c_{ij}}(t)$ is the dynamic corner frequency of ij^{th} subfault where $f_{c_{ij}}(t) = N_R(t)^{-1/3}4.9\times10^6\beta\left(\frac{\Delta\sigma}{M_{0_{ave}}}\right)^{1/3}$. Here $\Delta\sigma$ is the stress drop, $N_R(t)$ is the cumulative number of ruptured subfaults at time t, and $M_{0_{ave}} = M_0/N$ is the average seismic moment of subfaults. R_{ij} is the distance from the observation point, $Q(f)$ is the quality factor, $G(R_{ij})$ is the geometric spreading factor, $A(f)$ is the site amplification term, and $e^{-\pi\kappa f}$ is a high-cut filter to include the spectral decay at high frequencies described with the κ factor of soils. H_{ij} is a scaling factor introduced to conserve the high-frequency spectral level of the subfaults.

Table 1. Model parameters used in the simulation of the 1939 Erzincan earthquake

Parameter	**Value**
Moment Magnitude	8.0
Hypocenter Location	39.8° N, 39.38° E
Hypocenter Depth	11.25 km
Depth to the Top of the Fault Plane	0 km (360 km of surface rupture was observed)
Fault Orientation	Strike: 108°, Dip: 90°
Fault Dimensions	Length: 360 km, Width: 25 km
Crustal Shear Wave Velocity	3700 m/s
Rupture Velocity	3000 m/s
Crustal Density	2800 kg/m^3
Stress Drop	120 bar
Quality Factor	$Q = 122\,f^{0.68}$
Geometrical Spreading	$R^{-1.0}$
Duration Model	$T = T_0 + 0.05R$
Windowing Function	Saragoni-Hart
Kappa Factor	Regional kappa model (κ_0=0.066)
Site Amplification Factors	Corresponding site amplifications at each node (Boore and Joyner 1997)

In this study, among the source parameters, fault geometry (dimensions and fault angles) is taken from previous studies including Barka (1996), Stein et al. (1997) and Gursoy et al. (2013). The moment magnitude (Mw) of the earthquake is estimated using an empirical relationship by Wells and Coppersmith (1994) that relates Mw to the surface rupture length. The stress drop of the earthquake is computed via an empirical correlation between stress drop and fault width proposed by Mohammadioun and Serva (2001). Random slip distributions are assumed on the fault. The path parameters in Erzincan region were validated in past studies mostly using the ground motion records of the 1992 earthquake (Askan et al., 2013; 2015 and 2017). Finally, amplifications at each site of interest are considered through the site amplification factors proposed by (Boore and Joyner 1997). At each simulation node, available information on site classes is used to model the corresponding site amplification factors. Table 1 lists all of the model parameters used in the simulation of the1939 Erzincan earthquake.

4. RESULTS AND VALIDATIONS

Simulations are performed at 250 nodes within the study area bounded by 39º-40ºN latitudes and 39º-40ºE longitudes. Since it is not possible to demonstrate all of the simulated time histories, the spatial distribution of Peak Ground Acceleration (PGA) and Peak Ground Velocity (PGV) within the study area are presented in Figures 2.a and 2b respectively. The historical city center experience much higher ground motion levels compared to the surrounding Northern and Southern regions. This is expected due to the closer distances from the fault plane as well as softer soil conditions in the historical city center. The historical city which was located about 4 km south of the current city center, is exposed to a PGA of 1.25g and PGV of 145 cm/s. These very high values definitely contain modelling errors yet the amplitudes in general explain the widespread damage in the region. The estimated PGA and PGV values in the current city center during the 1939 event are 1g and 90 cm/s, respectively. The acceleration and velocity time histories along with the Fourier Amplitude Spectrum (FAS) of acceleration at these two selected nodes are displayed in Figures 3.a and 3.b: very high amplitudes of both acceleration and velocity are observed. The multiple wave packages on both acceleration time histories indicate finite-fault source effects radiating from the large fault plane.

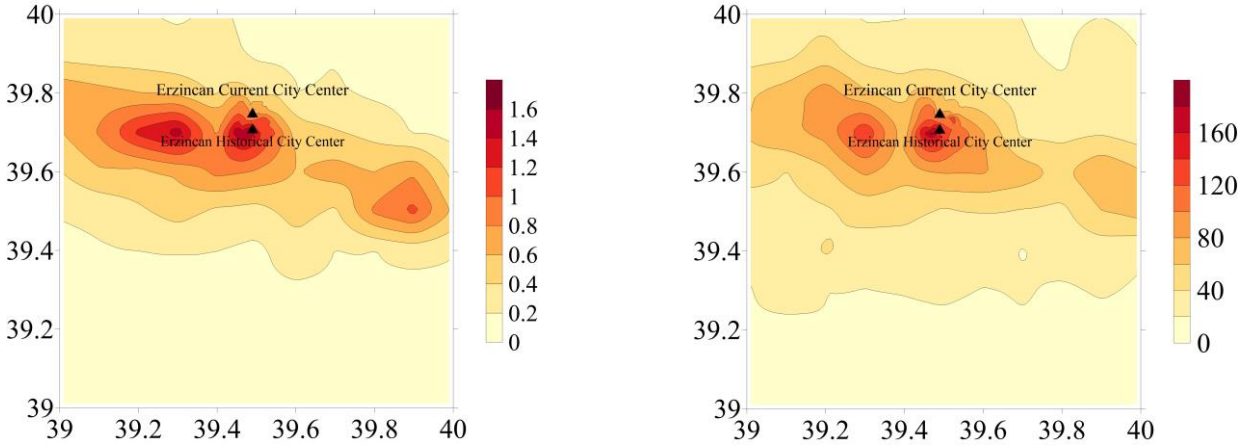

(a) (b)

Figure 2. Spatial distribution of the simulated (a) PGA (g), (b) PGV (cm/s) values of the 1939 Erzincan earthquake in Erzincan region

To check whether the simulations are modeled physically, the attenuation of the synthetic ground motion peaks is compared against the Ground Motion Prediction Equations (GMPEs) proposed by Boore and Atkinson (2008) and Akkar and Cagnan (2010) in Figure 4. These equations were previously shown to represent the attenuation characteristics in Eastern Turkey (Akansel et al., 2014). It is observed in Figure 4 that the simulated motions remain within ±1σ of both GMPEs indicating effectiveness of the simulations. Simulated data shows a more similar trend to the GMPE by Boore and Atkinson (2008).

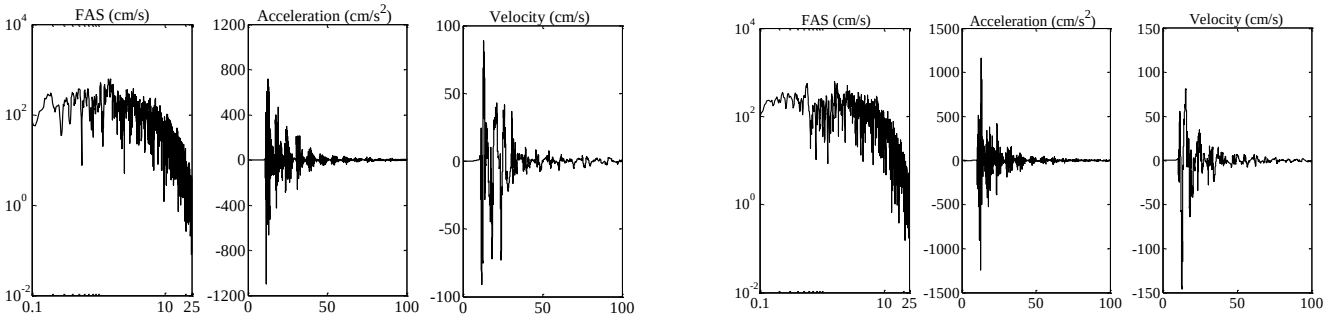

Figure 3. Simulated FAS, acceleration and velocity time histories in the (a) current Erzincan city center (ERC station) (b) historical Erzincan city center during the 1939 earthquake

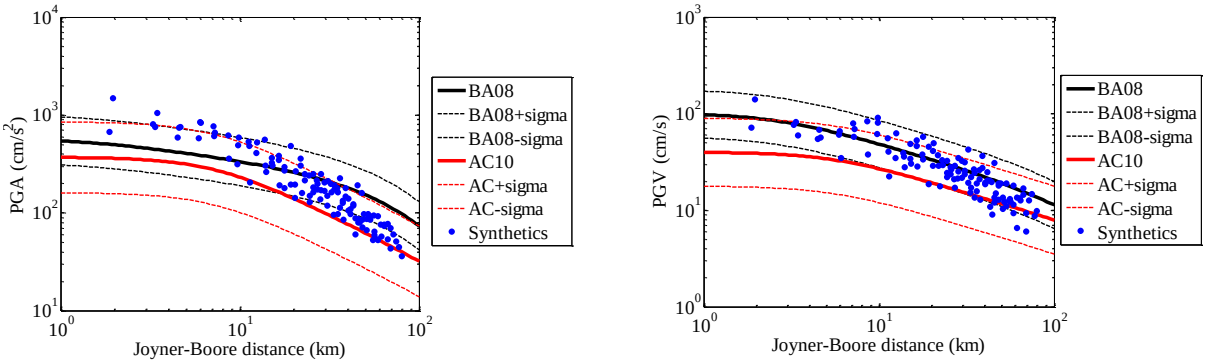

Figure 4. Attenuation of the simulated (a) PGA (b) PGV values at the selected nodes in comparison with the selected GMPEs by Boore and Atkinson (2008), BA08 and Akkar and Cagnan (2010), AC10

Since a direct validation of the simulation results is not possible due to lack of recorded motions of the 1939 Erzincan event, comparisons of the estimated intensity distribution with the observed one are presented. For this purpose, anticipated intensity values are computed at the nodes using local correlations between Modified Mercalli Intensity (MMI) and PGA as well as PGV derived for Turkey. The damage patterns monitored in the past earthquakes in Turkey reveal the importance of using local intensity models in terms of PGA and PGV for stiff structures and flexible structures, respectively (Erberik, 2008a; 2008b). Thus, the simulated PGA and PGV values at each node within the study area are used as inputs to the following simple linear relationships proposed by Bilal and Askan (2014):

$$MMI = 0.132 + 3.884 * \log(PGA) \quad (2)$$

$$MMI = 2.673 + 4.340 * \log(PGV) \quad (3)$$

Figure 5.a displays the observed intensity distribution collected in the field after the 1939 event in Medvedev–Sponheuer–Karnik (MSK) scale. It is known that the large intensity values in MSK and MMI scales correspond to the same felt intensity levels (Musson et al., 2010). Thus, the comparisons in MSK and MMI scales are considered to contain negligible error. Figures 5.b and 5.c display the estimated MMI values for the 1939 earthquake from Equation (2) and (3) using simulated motions, respectively. Comparison of the observed and estimated intensity values in the region reveals the consistency among them regardless of the relationship used. This consistency is much more obvious for both historical and current Erzincan city centers. Despite a slight overestimation of the observed intensity values in the Southern regions, the pattern of the simulated intensity distribution matches the observed one closely. This indicates a physically reasonable source, propagation and site

modeling in spite of the existing uncertainties and lack of data. In general, simulated motions are considered to conservatively estimate the anticipated ground motions of the 1939 Erzincan earthquake. The numerical results indicate that the levels of the ground motions were excessively large which explains the extent of the damage and number of fatalities in the event.

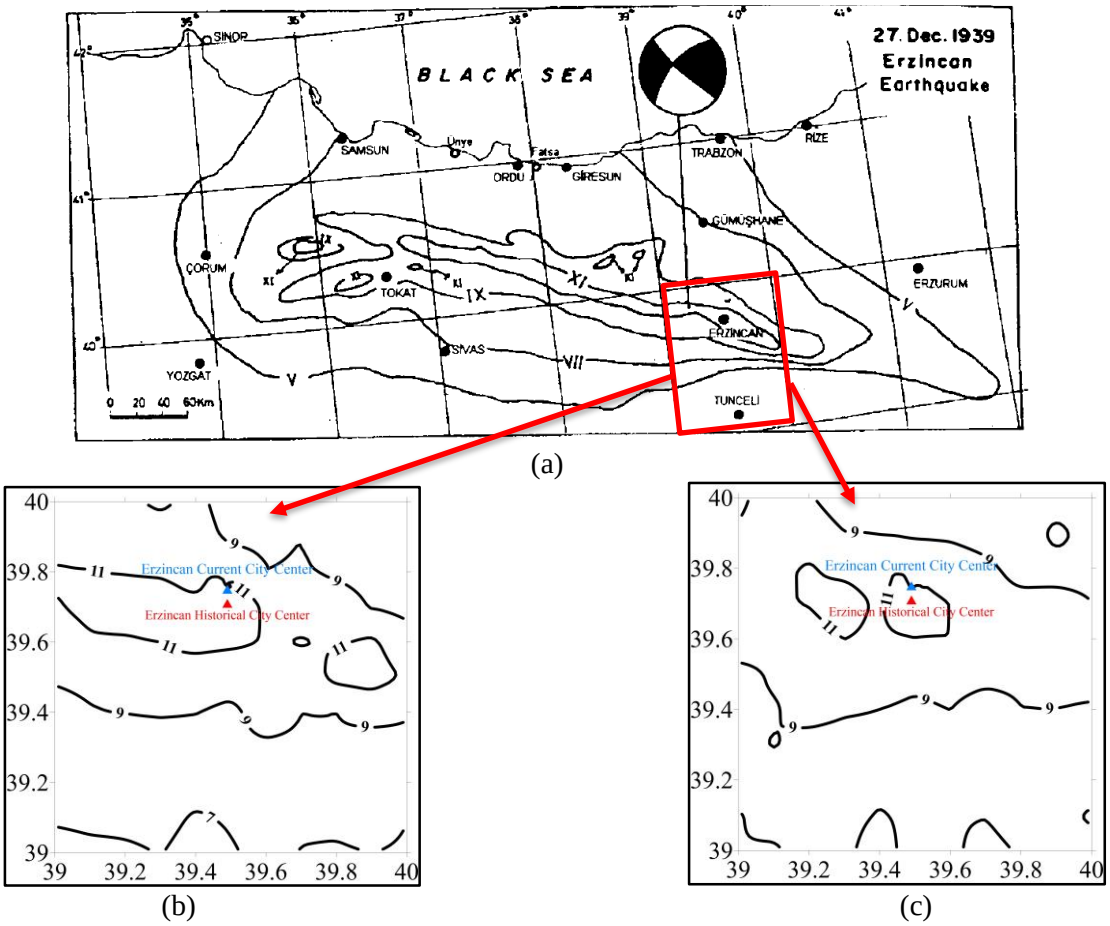

Figure 5. (a) Observed seismic intensity map of the 1939 Erzincan earthquake (Altinok and Ersoy, 2000); Estimated intensity distribution using (b) MMI-PGA correlation given in Equation (2), (c) MMI-PGV correlation given in Equation (3). The red box in (a) shows the study area as plotted in (b) and (c).

5. CONCLUSIONS

In this paper, the 1939 Erzincan (Ms~7.8) earthquake is studied through stochastic finite-fault ground motion simulations. The source parameters are estimated using empirical relationships and previous studies including observations on the fault plane. The path and site parameters are adapted from past studies in the region performed mostly with data from the 1992 Erzincan earthquake. A total of 250 nodes are selected in an area covering the historical and current Erzincan city centers.

The simulation results yield PGA and PGV values that exceed 1g and 100 cm/s, respectively at several nodes within the study area including the old and current city centers. The high amplitudes and spatial distribution of the simulated ground motions are consistent with the widespread damage observed during the 1939 event. To validate the simulations indirectly, observed intensity distribution after the earthquake is compared with the estimated ones. The estimated intensities are obtained using local empirical conversion relationships between MMI and PGA as well as PGV. The amplitudes and the pattern of the estimated intensities closely match the observed values. This

indicates a physically reasonable source, propagation and site modeling of the 1939 Erzincan earthquake despite the existing uncertainties and lack of data. In general, simulated ground motions and estimated intensities seem to explain the extent of the observed damage and losses in this historical event. This finding indicates that it is possible to study historical events with careful selection of model parameters despite existence of certain modeling assumptions and the corresponding errors.

Finally, relatively lower ground motion amplitudes and intensities are observed in the current city center as compared to those in the historical one. This could also explain why the Erzincan city was relocated to the North after the 1939 event. Yet, after 53 years, the 1992 Erzincan (Mw=6.6) earthquake occurred on NAFZ, this time close to the current city center, causing again widespread damage and losses. This points out the importance of good construction practice in addition to an effective city planning that considers interdisciplinary knowledge for risk mitigation purposes.

REFERENCES

Akansel V., Ameri G., Askan A., Caner A., Erdil B., Kale Ö. and Okuyucu, D. (2014). The 23 October 2011 M W 7.0 Van (Eastern Turkey) earthquake: Interpretations of recorded strong ground motions and post-earthquake conditions of nearby structures. *Earthquake Spectra* **30:2**, 657-682.

Akkar, S. and Cagnan, Z. (2010). A local ground-motion predictive model for Turkey, and its comparison with other regional and global ground-motion models. *Bulletin of the Seismological Society of America* **100:6**, 2978-2995.

Altinok, Y. and Ersoy, S. (2000). Tsunamis observed on and near the Turkish coast. *Natural Hazards* **21**, 185-205.

Ambraseys, N.N. (1970). Some characteristic features of the North Anatolian Fault Zone. *Tectonophysics* **9(2-3),** 143-165.

Armijo, R., Meyer, B., Navarro, S., King, G., and Barka A. (2002). Asymmetric slip partitioning in the Sea of Marmara pull-apart: A clue to propagation processes of the North Anatolian Fault. *Terra Nova* **14:2**, 80-86.

Askan A., Karimzadeh S. and Bilal M. (2017). Seismic intensity maps for North Anatolian Fault Zone (Turkey) based on recorded and simulated ground motion data, Book Chapter, Neotectonics and Earthquake Potential of the Eastern Mediterranean Region, AGU Books, (Editors: Ibrahim Cemen, Yucel Yilmaz), Wiley, ISBN: 978-1-118-94498-1.

Askan A., Karimzadeh S., Asten M., Kılıç N., Şişman F.N. and Erkmen C. (2015). Assessment of seismic hazard in Erzincan (Turkey) region: construction of local velocity models and evaluation of potential ground motions. *Turkish Journal of Earth Sciences* **24:6**, 529-565.

Askan, A., Sisman, F.N. and Ugurhan, B. (2013). Stochastic strong ground motion simulations in sparsely-monitored regions: A validation and sensitivity study on the 13 March 1992 Erzincan (Turkey) earthquake. *Soil Dynamics and Earthquake Engineering* **55**, 170-181.

Avsar, U., Turkoglu, E., Unsworth, M., Caglar, I. and Kaypak, B. (2013). Geophysical images of the North Anatolian Fault Zone in the Erzincan Basin, Eastern Turkey, and their tectonic implications. *Pure and Applied Geophysics* **170:3**, 409-431.

Barka, A. (1992). The North Anatolian Fault Zone. *Annales tectonicae* **6**, 164-195.

Barka, A. (1993). The tectonics of Erzincan basin and 13 March 1992 Erzincan earthquake, Proceedings of the 2nd Turkish National Earthquake Engineering Conference, 259-270, Istanbul Technical University Structures and Earthquake Applications-Research Center, (in Turkish).

Barka, A. (1996). Slip distribution along the North Anatolian fault associated with the large earthquakes of the period 1939 to 1967. *Bulletin of the Seismological Society of America* **86(5)**, 1238– 1254.

Beresnev I., Atkinson G. (1997). Modeling finite-fault radiation from the ωn spectrum. *Bulletin of the Seismological Society of America* **87:1**, 67-84.

Bernard, P., Gariel, J.C. and Dorbath, L. (1997). Fault location and rupture kinematics of the magnitude 6.8, 1992 Erzincan earthquake, Turkey, from strong ground motion and regional records. *Bulletin of the Seismological Society of America* **87:5**, 1230–1243.

Bilal, M. and Askan, A. (2014). Relationships between felt ıntensity and recorded ground-motion parameters for Turkey. *Bulletin of the Seismological Society of America* **104**, 484–496.

Boore D.M. and Atkinson G.M. (2008). Ground-motion prediction equations for the average horizontal component of PGA, PGV, and 5% damped PSA at spectral periods between 0.01 sand 10.0s. *Earthquake Spectra* **24:1**, 99–138.

Boore, D.M. (1983). Stochastic simulation of high-frequency ground motions based on seismological models of the radiated spectra. *Bulletin of the Seismological Society of America* **73:6A**, 1865–1894.

Boore, D.M. and Joyner, W.B. (1997). Site amplifications for generic rock sites. *Bulletin of the seismological society of America* **87:2**, 327-341.

Castro, R.R., Rovelli A., Cocco M., Di Bona M. and Pacor F. (2001). Stochastic simulation of strong-motion records from the 26 September 1997 (Mw 6), Umbria–Marche (central Italy) earthquake. *Bulletin of the Seismological Society of America* **91:1**, 27–39.

Erberik, M.A. (2008a). Generation of fragility curves for Turkish masonry buildings considering in-plane failure modes. *Earthquake Engineering & Structural* Dynamics **37:3**, 387–405.

Erberik, M.A. (2008b). Fragility-based assessment of typical mid-rise and low-rise RC buildings in Turkey. *Engineering Structures* **30:5**, 1360–1374.

Frankel, A. (1993). Three-dimensional simulations of the ground motions in the San Bernardino valley, California, for hypothetical earthquakes on the San Andreas fault. *Bulletin of the Seismological Society of America* **83:4**, 1020-1041.

Gursoy, H., Tatar, O., Akpınar, Z., Polat, A., Mesci, L. and Tunçer, D. (2013). New observations on the 1939 Erzincan Earthquake surface rupture on the Kelkit Valley segment of the North Anatolian Fault Zone, Turkey. *Journal of Geodynamics* **65**, 259-271.

Karimzadeh S., Askan A. and Yakut A. (2017b). Assessment of simulated ground motions for their use in structural engineering practice; a case study for Duzce (Turkey). *Pure and Applied Geophysics*, DOI: 10.1007/s00024-017-1602-2.

Karimzadeh S., Askan A., Yakut A. and Ameri G. (2017a). Assessment of Alternative Simulation Techniques in Nonlinear Time History Analyses of Multi-Story Frame Buildings: A Case Study. *Soil Dynamics and Earthquake Engineering* **98**, 38-53.

Mohammadioun B. and Serva L. (2001). Stress drop, slip type, earthquake magnitude, and seismic hazard. *Bulletin of the seismological society of America* **91:4**, 694-707.

Motazedian, D. and Atkinson G.M. (2005). Stochastic finite-fault modeling based on a dynamic corner frequency, *Bulletin of the Seismological Society of America* **95:3**, 995–1010.

Motazedian, D. and Moinfar A. (2006). Hybrid stochastic finite fault modeling of 2003, M 6.5, Bam, earthquake (Iran). *Journal of Seismology* **10:1**, 91–103.

Musson, R.M.W., Grünthal, G. and Stucchi, M. (2010). The Comparison of Macroseismic Intensity Scales. *Journal of Seismology* **14:2**, 413-428.

Olsen, K.B., Archuleta, R.J. and Matarese, J.R. (1996). Three-dimensional simulation of a magnitude 7.75 earthquake on the San Andreas fault. *Science* **270:8**, 1628-1632.

Stein, R.S., Barka, A. and Dieterich, J.H. (1997). Progressive failure on the North Anatolian fault since 1939 by earthquake stress triggering. *Geophysical Journal International* **128:3**, 594-604.

Wells D. and Coppersmith K. (1994). New empirical relationships among magnitude, rupture length, rupture width, rupture area, and surface displacement. *Bulletin of the Seismological Society of America* **84:4,** 974-1002.